

Strong-field Control of the Z -Boson resonance in e^+e^- collisions

Fengye Chen, Qingzheng Lv,^{*} and Libin Fu[†]

Graduate School of China Academy of Engineering Physics,

100193 Beijing, People's Republic of China

(Dated: June 11, 2026)

arXiv:2606.09394v2 [hep-ph] 10 Jun 2026

Abstract

Resonant Z -boson production is a cornerstone of precision electroweak physics, with its vacuum line shape set by the Z mass, width, and collision kinematics. We show that a strong laser field can significantly alter this picture. By treating the field nonperturbatively, we find that laser dressing of the incoming fermions alters the effective collision kinematics and opens laser-photon exchange channels, including multiphoton processes, in e^+e^- collisions. As a result, the Z -resonance profile develops distinct intensity-dependent regimes, evolving from the vacuum limit to saturation at intermediate field strengths and to an approximately quadratic enhancement at higher intensities. Additionally, the polarization composition of the produced Z bosons is redistributed. In particular, at high intensities the laser-induced contribution can compensate the intrinsic chiral asymmetry of the electroweak interaction, leading to nearly parity-balanced Z -boson production. Our results identify that strong classical fields can dynamically control electroweak resonance phenomena, opening a bridge between strong-field QED and high-energy collider physics.

Resonant production of the Z boson in e^+e^- annihilation is central to precision electroweak physics, enabling some of the most stringent tests of the Standard Model [1, 2]. Measurements at the Z pole have established the chiral structure of neutral-current interactions [1, 3], constrained electroweak radiative corrections [2, 4], and enabled high-precision determinations of fundamental parameters through the resonance line shape, decay width, and polarization observables [2]. Owing to its sensitivity to both collision kinematics and coupling structure, the Z resonance also remains a powerful probe of possible physics beyond the Standard Model [5, 6]. External control over its line shape and polarization composition would therefore provide a new handle on precision electroweak measurements.

In the traditional vacuum picture, however, the structure of a resonance is largely fixed by the underlying quantum field theory [7], while external control is essentially limited to the choice of initial-state kinematics [8]. As a result, observables such as the resonance profile, production rate, and polarization composition are not independently tunable once the collision setup is specified. Exploring qualitatively different regimes of resonance dynamics therefore typically requires substantial changes in accelerator design or beam conditions [9–11]. This raises a basic question: can resonance phenomena themselves be dynamically reshaped by external fields, rather than merely probed through them?

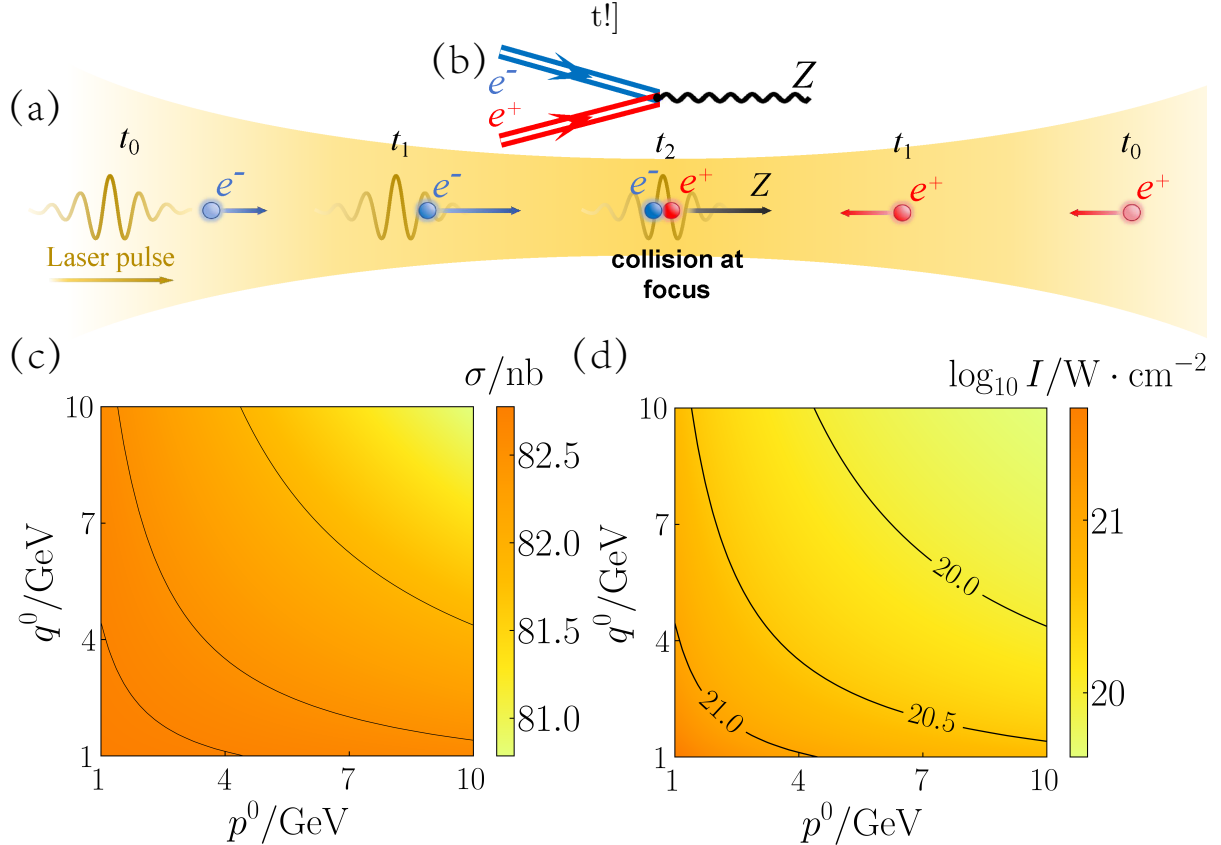


FIG. 1. (a) Schematic of the proposed e^+e^- collision geometry in a strong laser field. The labels t_0 , t_1 , and t_2 denote the initial state, the laser-induced dressing and acceleration of the electron, and the collision at the laser focus, respectively. The positron propagates with nearly constant energy before the collision [25]. (b) Feynman diagram for the dominant laser-assisted channel for resonant Z -boson production. Double solid lines denote laser-dressed (Volkov) electron and positron states. (c) Threshold laser intensity required to reach $\sqrt{s} = 91.2$ GeV as a function of the initial lepton energies. (d) Corresponding Z -boson production cross section for the parameters in (c). Contours indicate the laser intensities mapped from panel (c).

A route to such control emerges when the scattering process occurs in the presence of a strong classical background field capable of exchanging energy and momentum with the incoming particles. In strong-field quantum electrodynamics (QED) [12–15], charged fermions undergo nonperturbative dressing by the background [16–18], acquiring field-dependent quasi-momenta and accessing laser-photon exchange channels, including multiphoton processes, that modify the structure of scattering amplitudes. Such effects are well established in purely electromagnetic processes, where they can strongly alter energy flow [19, 20], spin transfer [21], and polarization observables [22–24]. Their implications for electroweak interactions, however, and in particular for resonant Z -boson production, remain largely

unexplored.

In this Letter, we show that nonperturbative laser dressing of the incoming fermions [16] can strongly reshape the Z -resonance profile in e^+e^- collision. This dressing modifies the effective collision kinematics and opens laser-photon exchange channels, causing the cross section to evolve from the vacuum behavior to saturation at intermediate field strengths and to an approximately quadratic scaling at high intensities. The strong-field background also redistributes the polarization composition of the produced Z bosons and can substantially reduce the net chiral asymmetry, driving the process toward nearly parity-balanced production at high intensities.

We consider an e^+e^- collision taking place within an intense laser pulse [Fig. 1(a)]. The electron beam co-propagates with the laser, while the positron beam collides head-on at the focal region where the field is strongest. In the background field, the incoming charged fermions are dressed by the laser and acquire a phase-dependent kinetic four-momentum [26]

$$P^\mu(\phi) = p^\mu - eA^\mu(\phi) + \left[\frac{e p \cdot A(\phi)}{2p \cdot k} - \frac{e^2 A^2(\phi)}{2p \cdot k} \right] k^\mu, \quad (1)$$

where p^μ is the asymptotic four-momentum, $k^\mu = \omega(1, 0, 0, 1)$ is the laser wave vector, and $A^\mu(\phi) = a_0(\epsilon^\mu e^{i\phi} + \text{c.c.})$ is the four-potential, which depends only on the phase $\phi = k \cdot x$. Here a_0 and ϵ^μ denote the field amplitude and polarization vector. This dressing induces a quasi-momentum shift of the incoming particles, thereby modifying the effective collision kinematics and enabling laser-assisted energy-momentum exchange during the collision process. Here and throughout, $a \cdot b = g_{\mu\nu} a^\mu b^\nu$ with metric signature $g_{\mu\nu} = \text{diag}\{+, -, -, -\}$, and natural units $\hbar = c = \epsilon_0 = 1$ are used.

We focus on a circularly polarized laser field, which suppresses off-resonant scattering while preserving the essential ponderomotive energy transfer [25]. A key feature of this geometry is that for co-propagating electrons the invariant $k \cdot p$ in the quasi-momentum becomes small, leading to a large ponderomotive contribution $\Delta^\mu(p) = e^2 a_0^2 k^\mu / (k \cdot p)$. The resulting enhancement of the effective center-of-mass energy is

$$\sqrt{s} = \sqrt{e^2 a_0^2 \left(\frac{p \cdot k}{q \cdot k} + \frac{q \cdot k}{p \cdot k} + 2 \right) + 2p \cdot q}, \quad (2)$$

where p^μ and q^μ denote the incident electron and positron four-momenta. This allows the

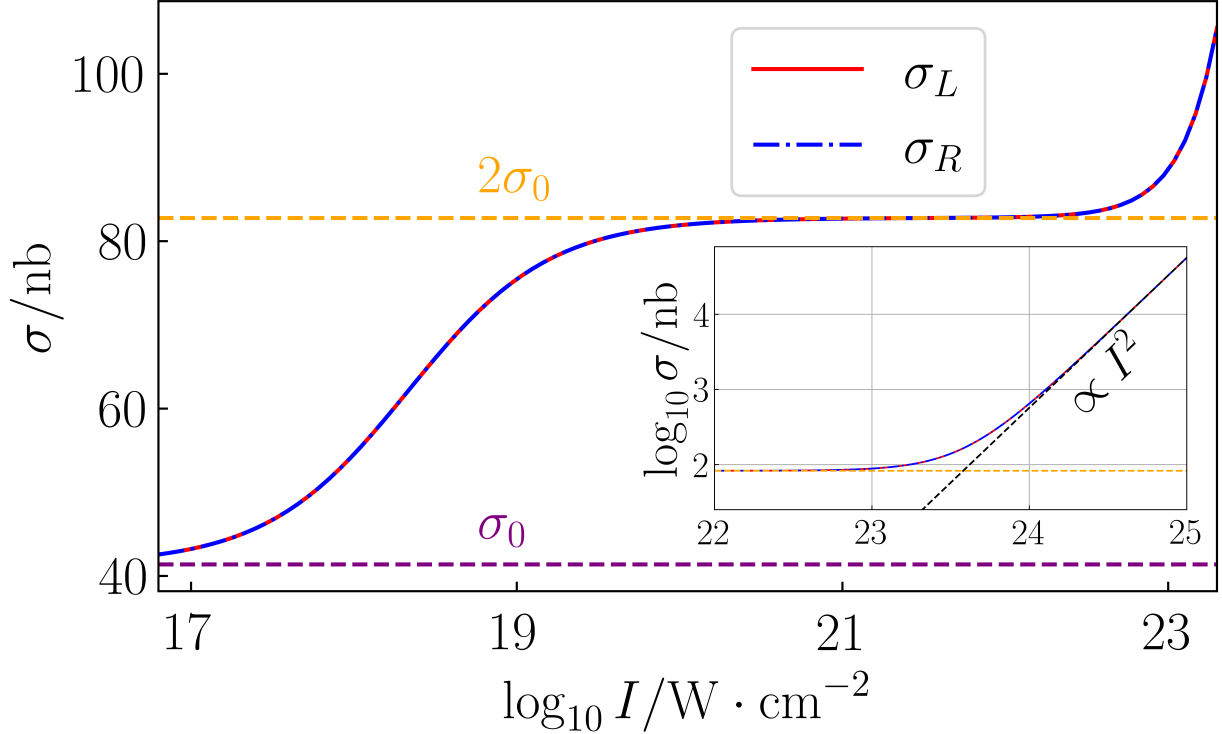


FIG. 2. Z -boson production cross section for equal initial lepton energies ($p^0 = q^0$) as a function of laser intensity. The results for left- and right-handed circular polarization overlap. For comparison, the field-free cross section is $\sigma_0 = 41.2$ nb [27], recovered from Eq. (7) in the limit $a_0 \rightarrow 0$.

system to reach the Z pole even with GeV-scale beams. For example, at laser intensities of order 10^{20} W/cm², the Z pole can be reached with beam energies as low as 6.6 GeV. Thus, strong-field dressing can dynamically realize a resonance condition that in vacuum is fixed solely by the beam energy; see Fig. S1 [25].

The laser intensity required to reach $\sqrt{s} = 91.2$ GeV in the laser-dressed kinematics is shown in Fig. 1(c) as a function of the initial beam energies. For currently accessible GeV-scale accelerators [28–30], the required intensities are 10^{20} – 10^{21} W/cm², within reach of present high-power laser facilities [31–36]. The resulting $e^+e^- \rightarrow Z$ cross section [Fig. 1(d)] can reach ~ 82.4 nb, about twice the vacuum Z -pole value [27]. Strong classical backgrounds can therefore compensate for the energy deficit of sub-resonant beams and substantially enhance the electroweak production rate.

This enhancement reflects two strong-field effects. The ponderomotive shift of the lepton quasi-momenta increases the effective invariant mass of the annihilating pair and enables access to the resonance, while nonperturbative dressing of the incoming fermions opens laser-photon exchange channels that further modify the production amplitude. The background

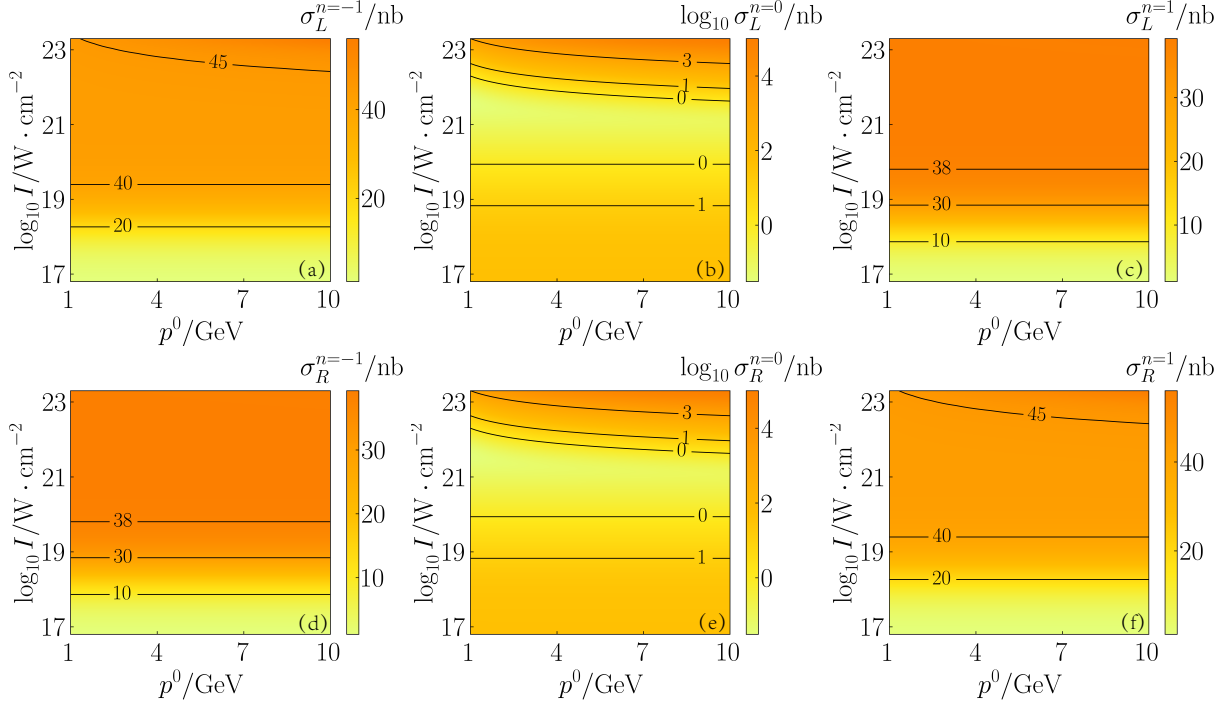


FIG. 3. Channel-resolved contributions to the total cross section as functions of the initial electron energy and laser intensity. Panels (a)–(c) correspond to a left-handed circularly polarized laser field, and panels (d)–(f) to the right-handed case. The labels $n = \{0, \pm 1\}$ denote the corresponding laser-photon exchange channels. The initial positron energy is chosen according to Eq. (2).

field thus acts as an active element of the electroweak scattering process.

We now analyze laser-assisted $e^+e^- \rightarrow Z$ production within the Furry picture [26, 37], treating the incoming leptons as Volkov states [Fig. 1(b)]. The system is governed by

$$\begin{aligned} \mathcal{L} = & \bar{\psi}(i\cancel{\partial} - m_e - e\cancel{A})\psi + \frac{1}{2}m_Z^2 Z^2 - \frac{1}{4}\mathcal{Z}^{\mu\nu}\mathcal{Z}_{\mu\nu} \\ & - \frac{g}{2\cos\theta_W}\bar{\psi}\cancel{Z}(2\sin^2\theta_W - P_L)\psi, \end{aligned} \quad (3)$$

where $\mathcal{Z}^{\mu\nu} = \partial^\mu Z^\nu - \partial^\nu Z^\mu$ with Z^μ being Z -boson field. The Z coupling retains its standard electroweak form, with $g = e/\sin\theta_W$ and $\sin^2\theta_W = 0.23$ [1], while $P_L = (1 - \gamma^5)/2$ reflects the chiral structure of the electroweak interaction. Since the laser couples only to the charged fermions, all strong-field corrections enter through the Volkov-dressed electron and positron states.

Strong-field dressing manifests at the amplitude level through a decomposition of the transition amplitude into photon-number channels. Within the Furry picture, the corresponding S -matrix element for an initial electron and positron with momenta p and q , and

spins s and s' , is

$$S_{fi} = -i \int d^4x \frac{g}{2 \cos \theta_W} \bar{\psi}_{q,s'}^p(x) \not{Z} (2 \sin^2 \theta_W - P_L) \psi_{p,s}^e(x). \quad (4)$$

The electron Volkov state in the plane-wave laser background is [16]

$$\psi_{p,s}^e(x) = \left(1 + \frac{e \not{k} \not{A}(x)}{2p \cdot k} \right) \frac{u_s(p)}{\sqrt{2P^0V}} e^{-iS_p(x)}, \quad (5)$$

with $S_p(x) = p \cdot x + \int d^4x \left[\frac{ep \cdot A(x)}{k \cdot p} - \frac{e^2 A(x)^2}{2k \cdot p} \right]$ is the laser-dressed phase and $(\not{p} - m)u_s(p) = 0$, while the positron state follows by charge conjugation. The plane-wave approximation is justified because the coherence length of the process is much shorter than the laser period [38].

The resulting S -matrix element takes the form,

$$S_{fi} = \sum_n (2\pi)^4 \delta^4(\kappa_n) \mathcal{M}_n, \quad (6)$$

where n is the net number of exchanged laser photons and $\kappa_n = p + \Delta(p) + q + \Delta(q) + nk - k_Z$, with k_Z the four-momentum of the produced Z boson. This decomposition makes the multiphoton structure induced by the strong classical background explicit.

The total cross section takes the form

$$\sigma = \frac{1}{4\sqrt{s} |\vec{p}_r|} \sum_{\text{spin}} \sum_n |\mathcal{M}_n|^2 \frac{1}{m_Z \Gamma_Z}, \quad (7)$$

where $|\vec{p}_r| = \sqrt{s - 4m_e^2}$. The finite width of the Z boson is included through the Breit-Wigner resonance profile [1, 27, 39, 40]. In the regime considered here, laser-induced modifications of the Z decay width are negligible because the dominant decay channels are essentially insensitive to the external field [25].

Figure 2 shows the total cross section as a function of laser intensity. In the weak-field regime ($\lesssim 10^{17}$ W/cm²), it reproduces the standard field-free Z -pole value, $\sigma_0 = 41.2$ nb [27], indicating that the laser has a negligible effect and the process reduces to conventional electroweak scattering in vacuum.

As the intensity increases to 10^{20} – 10^{22} W/cm², the cross section enters a saturation regime and forms a plateau near $2\sigma_0$. This behavior reflects the onset of laser-assisted

channels whose contribution becomes comparable to the field-free one, redistributing the scattering probability across different photon-number pathways.

At still higher intensities ($\gtrsim 10^{23}$ W/cm²), the cross section crosses over to an approximately quadratic growth with laser intensity, signaling the onset of a strongly nonlinear regime. The sequence of vacuum-like behavior, saturation, and nonlinear enhancement shows that strong classical backgrounds qualitatively reshape electroweak scattering rather than merely providing a perturbative correction.

To understand the intensity dependence and the competition between photon-exchange channels, we examine the channel-resolved amplitudes \mathcal{M}_n , defined by

$$\mathcal{M}_n = -\frac{ig}{2 \cos \theta_W} \bar{v}_{s'}(q) \mathcal{F}_n^\lambda u_s(p). \quad (8)$$

Here \mathcal{F}_n^λ encodes the laser-dressed interaction, where λ labels the polarization of the produced Z boson [41]. In general, it contains terms proportional to Bessel functions $J_n(\alpha)$, reflecting the exchange of n laser photons and thereby the multiphoton character of the process [25]. The parameter $\alpha = ea_0 \left| \frac{p \cdot \epsilon}{p \cdot k} - \frac{q \cdot \epsilon}{q \cdot k} \right|$ controls the strength of the laser-induced coupling.

For a circularly polarized laser with collinear beams, $p \cdot \epsilon = q \cdot \epsilon = 0$, so that $\alpha = 0$. The dynamics are then dominated by the lowest-order channels $n = 0, \pm 1$, while higher-order contributions are kinematically suppressed. In this limit, the dynamics are fully captured by the matrices $\mathcal{F}_{0,\pm 1}^\lambda$,

$$\mathcal{F}_{-1}^\lambda = \frac{ea_0}{2p \cdot k} G^\lambda \not{k} \not{\epsilon}^* - \frac{ea_0}{2q \cdot k} \not{\epsilon}^* \not{k} G^\lambda, \quad (9)$$

$$\mathcal{F}_0^\lambda = G^\lambda + \frac{e^2 a_0^2}{4(q \cdot k)(p \cdot k)} (\not{k} \not{\epsilon} G^\lambda \not{k} \not{\epsilon}^* + \not{k} \not{\epsilon}^* G^\lambda \not{k} \not{\epsilon}), \quad (10)$$

$$\mathcal{F}_1^\lambda = \frac{ea_0}{2p \cdot k} G^\lambda \not{k} \not{\epsilon} - \frac{ea_0}{2q \cdot k} \not{\epsilon} \not{k} G^\lambda. \quad (11)$$

Here, $G^\lambda = \not{\epsilon}_Z^\lambda (2 \sin^2 \theta_W - P_L)$ [25]. The behavior shown in Fig. 2 arises from the competition between these different channels. To further elucidate this, Fig. 3 decomposes the total cross section into the $n = 0$ and $n = \pm 1$ contributions, as a function of laser intensity and initial beam energy.

In the vacuum-like limit (laser intensity $\lesssim 10^{17}$ W/cm²), only the leading term in \mathcal{F}_0^λ

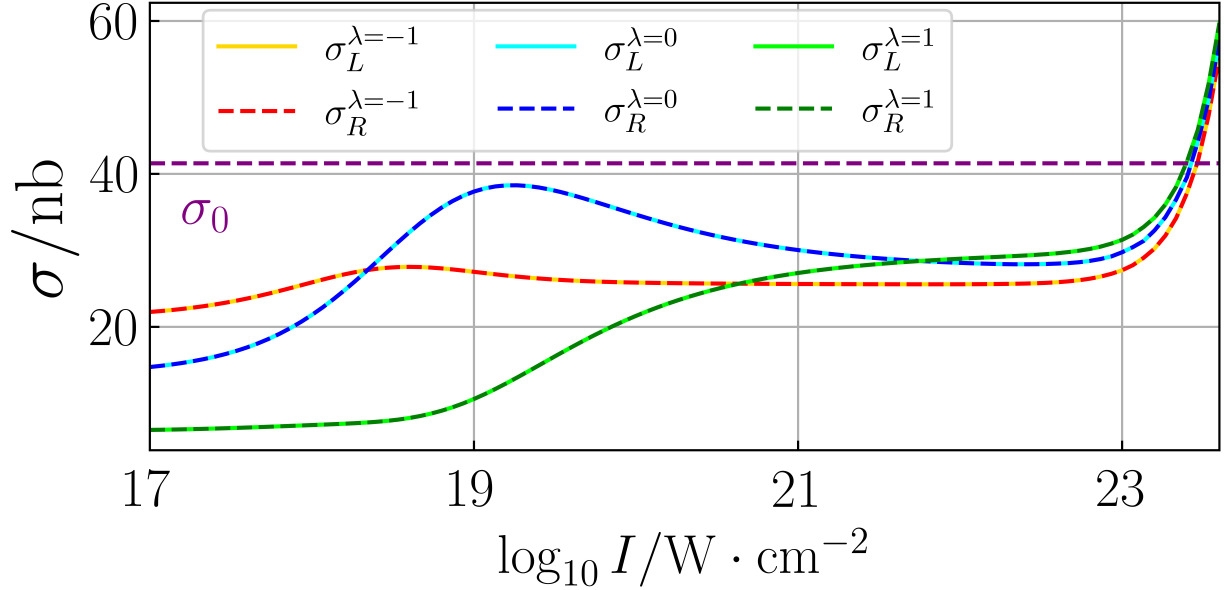


FIG. 4. Cross sections for the different polarization states of the produced Z boson ($\lambda = -1, 0, 1$) as functions of laser intensity. The initial lepton energies are taken to be equal, $p^0 = q^0$, according to Fig. 1(c).

survives, recovering the standard vacuum cross section σ_0 [Fig. 3(b,e)]. As the laser intensity increases, the single-photon channels $\mathcal{F}_{\pm 1}^\lambda$ grow linearly with the field amplitude a_0 through the prefactors $ea_0/(2p \cdot k)$ and $ea_0/(2q \cdot k)$ [Fig. 3(a,d) and (c,f)] and become comparable to the $n = 0$ contribution. The resulting channel competition redistributes the scattering probability and produces a saturation plateau near $2\sigma_0$.

At high intensities ($\gtrsim 10^{23}$ W/cm 2), the a_0^2 term in \mathcal{F}_0^λ dominates [Fig. 3(b,e)]. Generated by the product of the Volkov dressing factors on the electron and positron states, these terms contribute already in the $n = 0$ channel, i.e., without net photon exchange, and drive the approximately quadratic growth of the total cross section with laser intensity. Strong-field modification therefore originates not only from explicit photon-exchange channels but also from intrinsic dressing of the scattering states.

The same channel structure also explains the symmetry of the total cross section under reversal of the helicity of the circularly polarized laser field [Fig. 2]. This invariance follows directly from the laser-dressed matrix elements in Eqs. (9)–(11): the polarization vectors for opposite laser helicities are related by complex conjugation, which leaves the $n = 0$ channel unchanged and interchanges the $n = \pm 1$ channels. The summed cross section is therefore insensitive to the laser helicity.

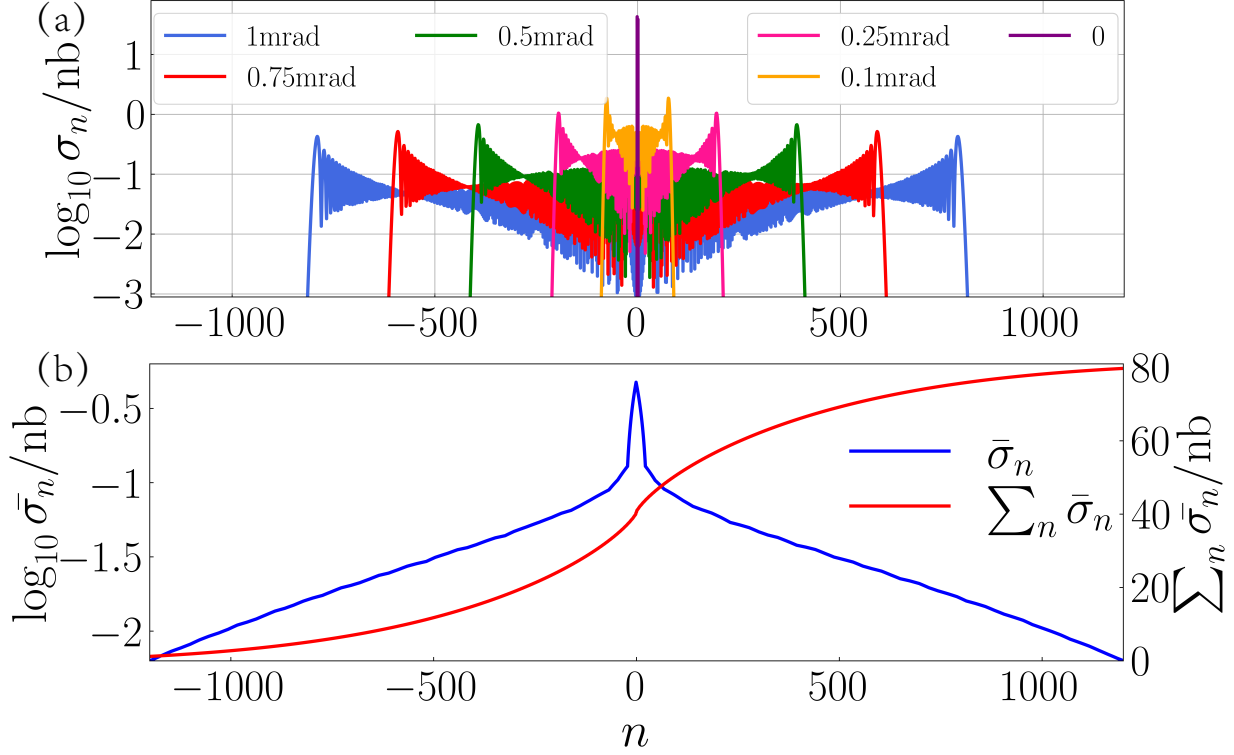


FIG. 5. (a) Channel-resolved cross sections for positron with incidence angle deviation $\Delta\theta_+ = 0, 0.1, 0.25, 0.5, 0.75,$ and 1 mrad, which simulate the scattering behavior of beam components with angular dispersion. (b) Channel-resolved cross section $\bar{\sigma}_n$ and cumulative cross section $\sum_n \bar{\sigma}_n$ for a representative beam with with angular dispersion of 1 mrad, obtained from Monte Carlo simulations. These two curves are respectively applicable to the coordinate axes on the left and right sides and the latter one is the cumulative sum of the former.

The polarization composition of the produced Z bosons, however, depends strongly on laser intensity [Fig. 4]. In the vacuum-like limit, the $\lambda = -1$ mode dominates, consistent with standard Z -pole production [1]. As the intensity increases to $\sim 10^{19}$ W/cm², the longitudinal component ($\lambda = 0$) becomes comparable and eventually dominant. This crossover is driven by the single-photon channels ($n = \pm 1$), whose matrix elements $\mathcal{F}_{\pm 1}^\lambda \propto \not{k}\not{\epsilon}$ induce spin-flip transitions in the leptonic current and relax the helicity selection rules that suppress longitudinal Z production in vacuum.

At still higher intensities ($\gtrsim 10^{23}$ W/cm²), the polarization asymmetry is strongly reduced and the produced Z bosons approach a nearly unpolarized mixture [Fig. 4]. This behavior is driven by the quadratic dressing contribution in \mathcal{F}_0^λ , which contains structures of the form $\not{k}\not{\epsilon} G^\lambda \not{k}\not{\epsilon}^*$ and its conjugate. These terms make the helicity contributions to the leptonic current increasingly symmetric, thereby reducing the net chiral asymmetry and driving the

Z -boson polarization toward approximate parity balance. Such strong-field control of the chiral asymmetry and polarization composition of the produced Z bosons is absent in the field-free process and opens a route to engineering electroweak final states with external classical backgrounds.

To assess the robustness of these effects under realistic conditions, we account for the finite energy spread and angular divergence of the incident beams. A relative energy spread of order $\Delta E/E \sim 10^{-3}$ [42–44] changes the dressed resonance condition only slightly. This effect can be compensated by a modest retuning of the laser intensity, indicating stability against typical beam-energy fluctuations [25]. Angular divergence is more important because noncollinear incidence ($p \cdot \epsilon \neq 0$, and hence $\alpha \neq 0$) activates additional photon-exchange harmonics. The effect is markedly different for the positron and electron beams. For positrons, mrad-level divergence [45] is well described by an incoherent sum over channels, and the overall enhancement remains largely preserved [Fig. 5]. Monte Carlo simulations confirm that the activated nonlinear channels add incoherently, leaving the channel-summed cross section nearly unchanged from the zero-divergence case. For electrons, by contrast, the small denominator $p \cdot k$ amplifies angular effects and weakens the ponderomotive shift, shifting the collision away from resonance and requiring either tighter alignment or higher peak laser intensity to compensate [25]. Even with these constraints, existing GeV-scale accelerators [28–30] combined with 10^{20} – 10^{22} W/cm² laser systems [31–36] can yield Z -boson production rates of over 10^9 events per year [25], indicating that laser-assisted collisions provide a complementary route toward compact electroweak platforms.

In conclusion, we have shown that an intense laser background can nonperturbatively reshape resonant Z -boson production in e^+e^- collisions through dressing of the initial states. Ponderomotive quasi-momentum shifts and laser-photon exchange channels together drive a characteristic evolution of the cross section from the vacuum-like limit to a saturation plateau and, at higher intensities, to a nonlinear growth regime. The same strong-field environment also redistributes the polarization composition of the produced Z bosons and can substantially reduce the net chiral asymmetry of the process. Our results show that resonance phenomena, usually fixed by intrinsic particle properties and beam kinematics, can be dynamically controlled by external classical fields, opening a complementary route to compact Z -mediated electroweak studies and revealing a direct connection between strong-field QED and high-energy resonance physics. Angular-momentum conservation further

suggests that multiphoton laser-assisted channels may imprint controllable orbital angular momentum on the produced Z bosons, providing an additional handle on electroweak final states.

This work was supported by the National Natural Science Foundation of China (Grants No. 12088101 and No. U2330401).

Supplemental Material

This supplementary material follows the same symbol rules and signs as the main text. Relativistic units with $\hbar = c = \varepsilon_0 = 1$ and the metric of space-time $g^{\mu\nu} = \text{diag}\{+, -, -, -\}$ are used throughout this supplementary material.

Classical dynamics of charged fermions in a strong laser field

From the Lorentz equation, the classical four-momentum of a charged fermion in a plane-wave laser field is [26]

$$P^\mu(\phi) = p^\mu - eA^\mu(\phi) + \left[\frac{ep \cdot A(\phi)}{p \cdot k} - \frac{e^2 A^2(\phi)}{2p \cdot k} \right] k^\mu, \quad (12)$$

where p^μ is the asymptotic four-momentum of the fermion, $k^\mu = \omega(1, 0, 0, 1)$ is the laser four-wavevector, and

$$A^\mu(\phi) = a_0(\epsilon^\mu e^{i\phi} + \text{c.c.}) \quad (13)$$

is the four-potential, which depends only on the laser phase $\phi = k \cdot x$. Here a_0 denotes the field amplitude and ϵ^μ the polarization four-vector.

For the configuration considered here, the electron beam co-propagates with the laser. In this case,

$$k \cdot p \approx \frac{m_e^2 k^0}{2p^0}, \quad (14)$$

so that the laser-induced adiabatic momentum shift,

$$\Delta^\mu(p) = \frac{e^2 a_0^2}{2k \cdot p} k^\mu \approx \frac{e^2 a_0^2 p^0}{m_e^2 k^0} k^\mu, \quad (15)$$

can become much larger than the initial electron energy scale p^0 . As a result, the laser dressing can strongly modify the effective collision kinematics.

In the center-of-mass frame of the laser-dressed incoming particles, defined by vanishing total three-momentum, the corresponding center-of-mass energy is

$$\sqrt{s} = \sqrt{2m_e^2 + 2[p + \Delta(p)] \cdot [q + \Delta(q)]}. \quad (16)$$

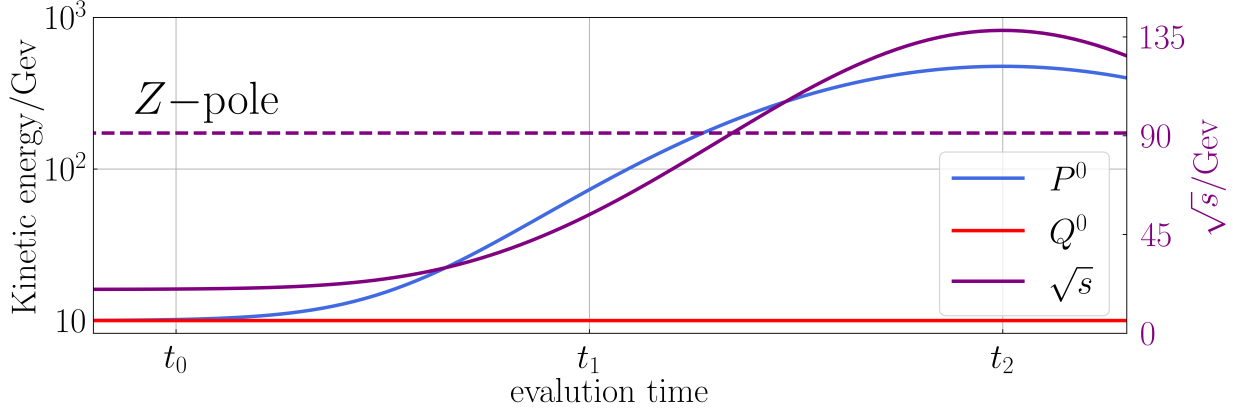


FIG. S6. Classical dynamics simulations of the electron and positron beam energies as functions of acceleration time at a laser intensity of 10^{20} W/cm². The initial energy of each beam is 10 GeV. The time markers t_0 , t_1 , and t_2 correspond to particle arrival at the beginning of the pulse, at the temporal midpoint of the pulse where the field amplitude is half of its peak value, and at the peak of the laser pulse, respectively. The corresponding center-of-mass energy is also shown for comparison. The Z -pole value is indicated by the dashed line.

Using the explicit form of the dressing-induced momentum shift, one obtains

$$\sqrt{s} \approx \sqrt{e^2 a_0^2 \left(\frac{p \cdot k}{q \cdot k} + \frac{q \cdot k}{p \cdot k} + 2 \right) + 2p \cdot q}. \quad (17)$$

In the collinear configuration, the dominant contribution arises from the strongly asymmetric factor

$$\frac{q \cdot k}{p \cdot k} \approx \frac{4p^0 q^0}{m_e^2}, \quad (18)$$

which can be very large. Therefore, even for moderate laser amplitudes, the laser-induced dressing can substantially enhance the effective center-of-mass energy.

To illustrate the laser-induced acceleration of the incoming particles, we simulate the classical dynamics of the electrons and positrons in the strong laser field. The time-dependent energy for the electrons (P^0) and positron (Q^0) as well as the center-of-mass energy \sqrt{s} is shown in Fig. S6. It shows that, for an initial beam energy of 10 GeV and a laser intensity of 10^{20} W/cm², the electron co-propagating with the laser experiences a pronounced energy boost during the interaction. As a result, the effective collision energy increases by nearly two orders of magnitude over the course of the laser pulse.

A central feature is that \sqrt{s} reaches, and subsequently exceeds, the Z -pole energy already before the laser field attains its peak amplitude. This demonstrates that the resonance

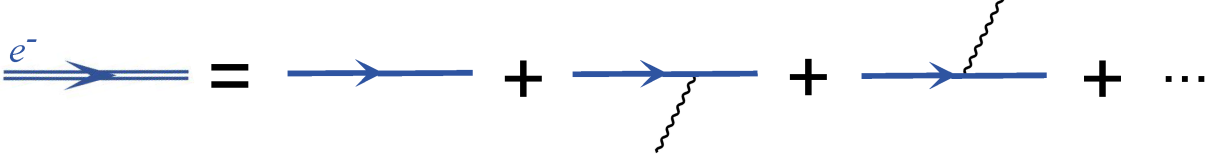


FIG. S7. Feynman diagram for an electron in the Furry picture. The double line denotes a laser-dressed electron (Volkov state), while the single line represents a bare electron. The diagram schematically depicts the expansion of the Volkov state into standard Feynman diagrams associated with multiple laser-photon interactions.

condition is not restricted to a single instant near the pulse maximum, but can instead be satisfied over an extended interval of the laser cycle. The region in which \sqrt{s} remains above the Z -pole therefore defines an effective collision window for resonant $e^+e^- \rightarrow Z$ production.

This effective window is important for two reasons. First, it shows that the laser-driven enhancement is sufficiently strong to bring the dressed collision energy into the electroweak resonance regime even when the initial beam energy is far below the vacuum threshold. Second, because the resonance condition is fulfilled over a finite temporal range rather than at a sharply isolated point, the collision setup is less sensitive to the precise timing of the interaction with respect to the pulse peak. In this sense, the off-peak resonant window provides a degree of robustness against timing jitter and pulse-shape variations, which is favorable for realistic implementations.

The dressing of the electrons and positrons in a strong laser field

The Volkov solution for an electron in a monochromatic plane-wave laser field can be written as [16]

$$\psi_{p,V}^e(x) = \frac{1}{\sqrt{2P^0V}} \left[1 + \frac{e\not{k}\not{A}(\phi)}{2p \cdot k} \right] u_r(p) e^{-iS_p(x)}, \quad (19)$$

where $\phi = k \cdot x$ is the laser phase, V is the normalization volume, and P^0 denotes the zeroth component of the laser-dressed four-momentum. The laser-dressed phase functions are $S_p(x) = p \cdot x + \int d^4x \left[\frac{ep \cdot A(x)}{k \cdot p} - \frac{e^2 A(x)^2}{2k \cdot p} \right]$ and the field-free bispinor fulfilling $(\not{p} - m) u_r(p) = 0$.

The corresponding Volkov solution for a positron $\psi_{p,V}^p(x)$ with same momentum is obtained by the substitutions $p^\mu \rightarrow -p^\mu$ and $u_s(p) \rightarrow v_s(p)$, with $v_s(p)$ being the field-free bispinor for positrons $(\not{p} + m) v_r(p) = 0$.

Taking the electron case as an example, the Volkov wave function in a monochromatic

plane-wave laser field can be expanded into harmonic components by means of the Jacobi–Anger expansion. One obtains

$$\begin{aligned}
\psi_{p,r}^e(x) &= \frac{1}{\sqrt{2P^0V}} \left[1 + \frac{ea_0 k}{2p \cdot k} (\not{\epsilon} e^{i\phi} + \not{\epsilon}^* e^{-i\phi}) \right] u_r(p) e^{-iP \cdot x} \sum_{n=-\infty}^{\infty} \mathcal{J}_n(\alpha, \beta) e^{-in(\phi+\theta)} \\
&= \frac{1}{\sqrt{2P^0V}} \sum_{n=-\infty}^{\infty} \left[\frac{ea_0 k \not{\epsilon}}{2p \cdot k} \mathcal{J}_{n-1}(\alpha, \beta) + \frac{ea_0 k \not{\epsilon}^*}{2p \cdot k} \mathcal{J}_{n+1}(\alpha, \beta) \right. \\
&\quad \left. + \mathcal{J}_n(\alpha, \beta) \right] u_r(p) e^{-iP \cdot x} e^{-in(\phi+\theta)},
\end{aligned} \tag{20}$$

and $P^\mu = p^\mu + \Delta^\mu(p)$ is the quasi-momentum showing above.

The above expansion follows from the generalized Jacobi–Anger identity

$$e^{-i\alpha \sin(\phi+\theta) + i\beta \cos 2\phi} = \sum_{n=-\infty}^{\infty} \mathcal{J}_n(\alpha, \beta) e^{-in(\phi+\theta)}, \tag{21}$$

where $\mathcal{J}_n(\alpha, \beta) = \sum_{n'=-\infty}^{\infty} J_{n-2n'}(\alpha) J_{2n'}(\beta)$ is the generalized Bessel function, with $J_n(x)$ the ordinary Bessel function of the first kind.

This harmonic decomposition shows that the Volkov state is a coherent superposition of components with phase factors $e^{-in\phi} = e^{-ink \cdot x}$. In momentum space, each harmonic therefore differs by an integer multiple of the laser four-momentum k^μ . Physically, the integer n labels the net number of laser photons exchanged between the charged particle and the background field. In the corresponding scattering amplitude, these harmonics appear as distinct laser-assisted channels, which can be represented diagrammatically as processes involving the absorption or emission of n laser photons, as illustrated in Fig. S7.

The parameters entering the generalized Bessel functions are determined by the laser field and the particle kinematics. The quantities

$$\alpha = ea_0 \frac{|p \cdot \epsilon|}{p \cdot k}, \quad \beta = e^2 a_0^2 \frac{|\epsilon^2|}{8p \cdot k} \tag{22}$$

characterize the nonlinear coupling between the particle and the laser. The parameter α is related to the angle between the particle momentum and the polarization of the laser, while the phase $\theta = \arg(p \cdot \epsilon)$ encodes the corresponding polarization-dependent phase shift. The parameter β originates from the quadratic term in the Volkov phase and depends on

the laser polarization. In particular, β vanishes for circular polarization, for which $\epsilon^2 = 0$, whereas it remains finite for linear or elliptical polarization.

Scattering Matrix Formulation of Resonant Z -Boson Production in a Strong Laser Field

Taking into account the nonperturbative dressing of the electron and positron in a strong laser field, the scattering matrix for the process depicted in Fig. 1(b) of the main text, with initial electron (positron) momentum p (q) and spin s (s'), is given by

$$\begin{aligned}
S_{fi} &= -\frac{ig}{2\cos\theta_W} \int d^4x \bar{\psi}_V^p \not{Z} (2\sin^2\theta_W - P_L) \psi_V^e \\
&= -\frac{1}{\sqrt{8P^0 Q^0 k_Z^0 V^3}} \frac{ig}{2\cos\theta_W} \int d^4x \bar{v}_{r'}(q) \left[1 + \frac{ea_0 \not{k}}{2p \cdot k} (\not{\epsilon} e^{i\phi} + \not{\epsilon}^* e^{-i\phi}) \right] \\
&\quad \not{\epsilon}_Z^\lambda (2\sin^2\theta_W - P_L) \left[1 + \frac{ea_0 \not{k}}{2p \cdot k} (\not{\epsilon} e^{i\phi} + \not{\epsilon}^* e^{-i\phi}) \right] u_r(p) e^{-iS_p^e(x) + iS_q^e(x) + ik_Z \cdot x} \delta_{r+r',\lambda} \quad (23) \\
&= -\frac{1}{\sqrt{8P^0 Q^0 k_Z^0 V^3}} \frac{ig}{2\cos\theta_W} \sum_{n=-\infty}^{\infty} \int \int d^4x \bar{v}_{r'}(q) \mathcal{F}_n^\lambda u_r(p) e^{-i\kappa \cdot x} \delta_{r+r',\lambda} \\
&= \frac{1}{\sqrt{8P^0 Q^0 k_Z^0 V^3}} \sum_{n=-\infty}^{\infty} (2\pi)^4 \delta^4(\kappa) \delta_{r+r',\lambda} \mathcal{M}_n,
\end{aligned}$$

where $\kappa = p + \Delta(p) + q + \Delta(q) + nk - k_Z$ with $\Delta^\mu(p) = e^2 a_0^2 k^\mu / (k \cdot p)$ and $\Delta^\mu(q) = e^2 a_0^2 k^\mu / (k \cdot q)$ being the ponderomotive shift for the electron and positron momentum, respectively. Here \mathcal{F}_n^λ is the coefficient for different production channels with exchanging photon number n , which can be fully expressed as

$$\begin{aligned}
\mathcal{F}_n^\lambda &= \frac{e^2 a_0^2}{4(q \cdot k)(p \cdot k)} \not{k} \not{\epsilon} G^\lambda \not{k} \not{\epsilon} \mathcal{J}_{n-2}(\alpha, \beta) e^{-i(n-2)\theta_\alpha} \\
&\quad + \left(\frac{ea_0}{2p \cdot k} G^\lambda \not{k} \not{\epsilon} + \frac{ea_0}{2q \cdot k} \not{k} \not{\epsilon} G^\lambda \right) \mathcal{J}_{n-1}(\alpha, \beta) e^{-i(n-1)\theta_\alpha} \\
&\quad + \left(G^\lambda + \frac{e^2 a_0^2}{4(q \cdot k)(p \cdot k)} \not{k} \not{\epsilon} G^\lambda \not{k} \not{\epsilon}^* + \frac{e^2 a_0^2}{4(q \cdot k)(p \cdot k)} \not{k} \not{\epsilon}^* G^\lambda \not{k} \not{\epsilon} \right) \mathcal{J}_n(\alpha, \beta) e^{-in\theta_\alpha} \quad (24) \\
&\quad + \left(\frac{ea_0}{2p \cdot k} G^\lambda \not{k} \not{\epsilon}^* + \frac{ea_0}{2q \cdot k} \not{k} \not{\epsilon}^* G^\lambda \right) \mathcal{J}_{n+1}(\alpha, \beta) e^{-i(n+1)\theta_\alpha} \\
&\quad + \frac{e^2 a_0^2}{4(q \cdot k)(p \cdot k)} \not{k} \not{\epsilon}^* G^\lambda \not{k} \not{\epsilon}^* \mathcal{J}_{n+2}(\alpha, \beta) e^{-i(n+2)\theta_\alpha}
\end{aligned}$$

where $G^\lambda = \not{\epsilon}_Z^\lambda (2 \sin^2 \theta_W - P_L)$. $\alpha = ea_0 |p \cdot \epsilon / p \cdot k - q \cdot \epsilon / q \cdot k|$ and $\beta = e^2 a_0^2 |\epsilon^2| (1/p \cdot k + 1/q \cdot k)$ are the arguments for the generalized Bessel function and $\theta_\alpha = \arg(p \cdot \epsilon / p \cdot k - q \cdot \epsilon / q \cdot k)$ is the phase. The index n represents the number of exchanged photons at the interaction vertices, which can be determined by the energy-momentum conservation.

When the laser is linearly polarized, the parameter β ensures that the Bessel function contributes significantly at the level of $n \sim \pm\beta$, which is proportional to a_0^2 . At high laser intensities, the factor β induces nonlinear effects that are more pronounced than those from α , leading to a significant deviation of the generated Z -bosons from the on-shell state. Consequently, selecting a circularly polarized laser is crucial, as the polarization vector satisfies $\epsilon^2 = 0$, resulting in $\beta = 0$. Furthermore, the circular polarization condition $\not{\epsilon}^2 = \epsilon^2 = 0$ eliminates both the first and last terms in Eq. (24), because of

$$\begin{aligned}
\not{k} \not{\epsilon} G^\lambda \not{k} \not{\epsilon} &= - \not{\epsilon} \not{k} G^\lambda \not{k} \not{\epsilon} \\
&= \not{\epsilon} G^\lambda \not{k} \not{k} \not{\epsilon} - 2(2 \sin^2 \theta_W - \frac{1}{2}) k \cdot \epsilon_Z^\lambda \not{k} \not{\epsilon} + i \not{\epsilon} \sigma^{\mu\nu} k_\mu \epsilon_{Z,\nu}^\lambda \gamma^5 \not{k} \not{\epsilon} \\
&= 2(2 \sin^2 \theta_W - \frac{1}{2}) k \cdot \epsilon_Z^\lambda \not{k} \not{\epsilon} \not{\epsilon} + \not{\epsilon} \gamma^5 \not{\epsilon}_Z^\lambda \not{k} \not{k} \not{\epsilon} - k \cdot \epsilon_Z^\lambda \not{\epsilon} \gamma^5 \not{k} \not{\epsilon} \\
&= - k \cdot \epsilon_Z^\lambda \gamma^5 \not{k} \not{\epsilon} \not{\epsilon} \\
&= 0.
\end{aligned} \tag{25}$$

with $k^2 = \not{k}^2 = 0$ and $k \cdot \epsilon = 0$. And, also the anticommutation relation $\{\not{\phi}, G^\lambda\} = 2(2 \sin^2 \theta_W - \frac{1}{2}) a \cdot \epsilon_Z^\lambda - i \sigma^{\mu\nu} a_\mu \epsilon_{Z,\nu}^\lambda \gamma^5$ for any slashed vector $\not{\phi}$ is used. It is the same for the case of polarized vector complex conjugate that $\not{k} \not{\epsilon}^* G^\lambda \not{k} \not{\epsilon}^* = 0$.

After accounting for these effects, the scattering coefficient \mathcal{F}_n^λ in a circularly polarized laser field can be expressed as

$$\begin{aligned}
\mathcal{F}_n^\lambda &= \left(\frac{ea_0}{2p \cdot k} G^\lambda \not{k} \not{\epsilon} + \frac{ea_0}{2q \cdot k} \not{k} \not{\epsilon} G^\lambda \right) J_{n-1}(\alpha) e^{-i(n-1)\theta_\alpha} \\
&+ \left[G^\lambda + \frac{e^2 a_0^2}{4(q \cdot k)(p \cdot k)} \not{k} \not{\epsilon} G^\lambda \not{k} \not{\epsilon}^* + \frac{e^2 a_0^2}{4(q \cdot k)(p \cdot k)} \not{k} \not{\epsilon}^* G^\lambda \not{k} \not{\epsilon} \right] J_n(\alpha) e^{-in\theta_\alpha} \\
&+ \left(\frac{ea_0}{2p \cdot k} G^\lambda \not{k} \not{\epsilon}^* + \frac{ea_0}{2q \cdot k} \not{k} \not{\epsilon}^* G^\lambda \right) J_{n+1}(\alpha) e^{-i(n+1)\theta_\alpha}.
\end{aligned} \tag{26}$$

Theoretical analysis of the enhancement in the cross section

When the collinear configuration is chosen, i.e., when the electron beam and the laser propagation direction are aligned, while the positron beam is counterpropagating, the condition $p \cdot \epsilon = 0$ leads to $\alpha = 0$ in the Bessel function, effectively suppressing nonlinear channels that involve the exchange of more than one photon. This simplifies the factor \mathcal{F}_n^λ to

$$\mathcal{F}_{-1}^\lambda = \frac{ea_0}{2p \cdot k} G^\lambda \not{k} \not{\epsilon}^* - \frac{ea_0}{2q \cdot k} \not{\epsilon}^* \not{k} G^\lambda, \quad (27)$$

$$\mathcal{F}_0^\lambda = G^\lambda + \frac{e^2 a_0^2}{4(q \cdot k)(p \cdot k)} \not{k} \not{\epsilon} G^\lambda \not{k} \not{\epsilon}^* + \frac{e^2 a_0^2}{4(q \cdot k)(p \cdot k)} \not{k} \not{\epsilon}^* G^\lambda \not{k} \not{\epsilon}, \quad (28)$$

$$\mathcal{F}_1^\lambda = \frac{ea_0}{2p \cdot k} G^\lambda \not{k} \not{\epsilon} - \frac{ea_0}{2q \cdot k} \not{\epsilon} \not{k} G^\lambda. \quad (29)$$

From Fig. 2 of the main text, it can be observed that once the laser intensity reaches $I \gtrsim 10^{21}$ W/cm², the total scattering cross section saturates at approximately $2\sigma_0$, where $\sigma_0 \approx 41.7$ nb is the standard vacuum cross section for resonant Z -boson production. In this regime, the process is dominated by the kinematic enhancement associated with the factor $(p \cdot k)^{-1}$ in the Volkov prefactor of Eq. (19). As a result, the dominant contributions arise from the first terms in Eqs. (27) and (29), and the scattering matrix may be approximated as

$$S_{fi} \approx - \frac{ig}{2 \cos \theta_W} \frac{ea_0}{2p \cdot k} \left\{ \bar{v}_{r'}(q) G^\lambda \not{k} \not{\epsilon}^* u_r(p) \delta^4[p + \Delta(p) + q + \Delta(q) - k - k_Z] \right. \\ \left. + \bar{v}_{r'}(q) G^\lambda \not{k} \not{\epsilon} u_r(p) \delta^4[p + \Delta(p) + q + \Delta(q) + k - k_Z] \right\}. \quad (30)$$

To make the helicity structure explicit, we adopt the Weyl representation of the Dirac matrices,

$$\gamma^0 = \begin{pmatrix} 0 & I_2 \\ I_2 & 0 \end{pmatrix}, \quad \gamma^1 = \begin{pmatrix} 0 & \sigma^1 \\ -\sigma^1 & 0 \end{pmatrix}, \quad \gamma^2 = \begin{pmatrix} 0 & \sigma^2 \\ -\sigma^2 & 0 \end{pmatrix}, \quad \gamma^3 = \begin{pmatrix} 0 & \sigma^3 \\ -\sigma^3 & 0 \end{pmatrix}. \quad (31)$$

Assuming that the laser propagates along the $+z$ direction with four-wavevector $k^\mu = \omega(1, 0, 0, 1)$, the operator products $\not{k} \not{\epsilon}$ for left- and right-circularly polarized photons take

the form

$$\not{k}\not{\epsilon}_L = 2\sqrt{2}\omega \begin{pmatrix} 0 & 0 & 0 & 0 \\ 1 & 0 & 0 & 0 \\ 0 & 0 & 0 & 0 \\ 0 & 0 & 0 & 0 \end{pmatrix}, \quad \not{k}\not{\epsilon}_R = -2\sqrt{2}\omega \begin{pmatrix} 0 & 0 & 0 & 0 \\ 0 & 0 & 0 & 0 \\ 0 & 0 & 0 & 1 \\ 0 & 0 & 0 & 0 \end{pmatrix}. \quad (32)$$

These operators act as helicity projectors and encode the angular-momentum selection rules associated with the single-photon-exchange channels $n = \pm 1$.

Consider, for example, a left-circularly polarized laser, corresponding to the $n = 1$ channel. The operator $\not{k}\not{\epsilon}_L$ selects the component of the spinor structure compatible with absorption of a photon carrying angular momentum -1 , thereby enforcing the corresponding helicity transition. In the ultrarelativistic limit $p^0 \gg m_e$, the relevant component of the electron spinor scales as $u(p) \sim m_e/\sqrt{2p^0}$. Using the kinematic approximation $p \cdot k \approx m_e^2\omega/(2p^0)$, the laser-assisted factor scales as

$$\frac{ea_0}{2p \cdot k} \not{k}\not{\epsilon}_L u(p) \sim \frac{ea_0}{m_e^2\omega} p^0 \cdot 2\sqrt{2}\omega \cdot \frac{m_e}{\sqrt{2p^0}} \approx \frac{2ea_0}{m_e} \sqrt{p^0}. \quad (33)$$

The required effective field strength is fixed by the ponderomotive threshold condition,

$$ea_0 = \sqrt{\frac{m_Z^2 - 2p \cdot q}{\frac{p \cdot k}{q \cdot k} + \frac{q \cdot k}{p \cdot k} + 2}} \approx m_Z \sqrt{\frac{p \cdot k}{q \cdot k}} \approx \frac{m_e m_Z}{2\sqrt{p^0 q^0}}, \quad (34)$$

where we have assumed $m_Z \gg p^0, q^0 \gg m_e$. Substituting Eq. (34) into the above estimate yields

$$\frac{ea_0}{2p \cdot k} \not{k}\not{\epsilon}_L u(p) \sim \frac{m_Z}{\sqrt{q^0}}. \quad (35)$$

Since the normalization of the positron spinor scales as $\bar{v}(q) \sim \sqrt{2q^0}$, the factor $1/\sqrt{q^0}$ in Eq. (35) cancels, resulting in an overall contribution of order m_Z . Consequently, once the laser intensity exceeds 10^{21} W/cm², the cross sections for the $n = \pm 1$ channels approach constants that are essentially independent of the laser intensity. This directly explains the plateau observed in Fig. 2 of the main text. Furthermore, this argument also shows that in the saturation regime, the scattering amplitude becomes insensitive to the incident beam energies (p^0 and q^0) at fixed laser intensity, consistent with the straight lines shown in Fig. 3 of the main text.

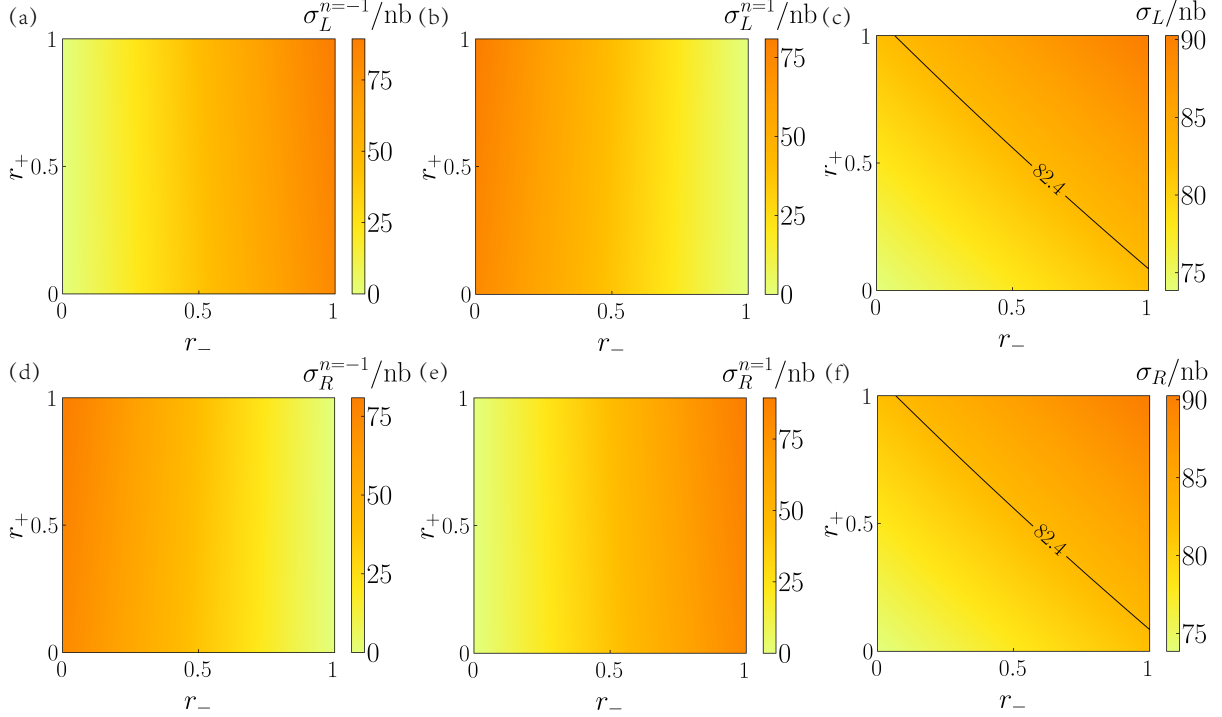


FIG. S8. Polarization effects on the cross sections. Panels (a) and (b) show the $n = \pm 1$ channel cross sections for a left-handed circularly polarized laser field, and panels (d) and (e) show the corresponding results for a right-handed field. Panels (c) and (f) display the total cross sections for the two sense of rotation directions of the laser field. Here, r_{\pm} denotes the polarization degree, defined as the fraction of incident particles with helicity $h = 1/2$ in the corresponding beam.

Including the spinor normalization explicitly, the laser-assisted interaction term approaches $\sqrt{2}m_Z$. By contrast, in the field-free process the corresponding spinor factor behaves as $\bar{v}_{s'}(q)u_s(p) \sim 2\sqrt{p^0q^0}$. Under the vacuum resonance condition $m_Z \approx 2\sqrt{p^0q^0}$, this factor is of order m_Z . Thus, the magnitude of the laser-assisted S -matrix element is enhanced by a factor of $\sqrt{2}$ relative to the vacuum case. The same reasoning applies symmetrically to the $n = -1$ channel with opposite photon helicity. Summing the $n = \pm 1$ contributions, and taking into account that only half of the unpolarized incident particles satisfy the relevant helicity selection rules in each channel, one finds that the total cross section approaches approximately twice the vacuum value.

We next comment on parity violation in the proposed collision scheme. In the derivation above, the incident spin states are summed over, which effectively averages over the chiral parity-violating factor P_L appearing in the electroweak vertex. This averaging removes the asymmetry from the total unpolarized expression, but the parity violation remains visible in the individual production channels. In particular, the difference between the $n = +1$ and

$n = -1$ channels is evident in Fig. S8[(a) and (b)] and [(d) and (e)].

Moreover, the individual $n = \pm 1$ channels exhibit a strong sensitivity to the polarization of the incident beams because of the angular-momentum transfer carried by the laser photons. The electron polarization is especially important, since the Volkov prefactor for electrons is much larger and therefore primarily determines whether the single-photon-assisted channel is efficiently accessed. This is fully consistent with the helicity selection rule encoded in Eq. (32). Although the total cross section remains symmetric, the polarized beams could in principle be used to selectively enhance or suppress specific channels. It should also be emphasized that the change in the total cross section induced by the incident polarization state, shown in Fig. S8(c) and (f), is caused by the parity-violating structure of the electroweak interaction.

When the laser intensity is increased further to $I \gtrsim 10^{23}$ W/cm², the Volkov prefactor $ea_0/(2q \cdot k)$ from positrons also becomes important. This happens because increasing the laser intensity not only increases a_0 , but also lowers the positron energy required to satisfy the resonance condition, thereby reducing $q \cdot k$. In this regime, the positron dressing produces two main effects. First, the second term in $\mathcal{F}_{\pm 1}^\lambda$ becomes non-negligible, although it remains smaller than the leading term. Second, the last two terms in \mathcal{F}_0^λ are strongly enhanced and begin to dominate the behavior of the $n = 0$ channel.

As an example, consider the second term in Eq. (28). Using the ultrarelativistic approximation $p \cdot k \approx 2p^0\omega$, the operator structure scales as

$$\frac{e^2 a_0^2}{4(p \cdot k)(q \cdot k)} \not{k} \not{\epsilon}^* G^\lambda \not{k} \not{\epsilon} \sim \frac{e^2 a_0^2 p^0}{2m_e^2 q^0} G^\lambda. \quad (36)$$

Here $\not{k} \not{\epsilon}^*$ and $\not{k} \not{\epsilon}$ correspond to two opposite photon-exchange processes, so that the net angular momentum transferred from the laser field vanishes. In this case, the Weyl-spinor components selected by angular-momentum conservation scale as

$$u_s(p) \sim \frac{m_e}{\sqrt{2p^0}}, \quad \bar{v}_{s'}(q) \sim \sqrt{2q^0}, \quad (37)$$

while the opposite scaling applies to the third term in Eq. (28). Using Eq. (34), the corre-

scattering matrix element behaves as

$$\frac{e^2 a_0^2}{4(p \cdot k)(q \cdot k)} \bar{v}(q) \not{k} \not{\epsilon}^* G^\lambda \not{k} \not{\epsilon} u(p) \sim e^2 a_0^2 \frac{m_Z}{2} \sqrt{\frac{p^0}{q^0}} G^\lambda. \quad (38)$$

This shows that the scattering amplitude in the $n = 0$ channel scales linearly with a_0^2 , and therefore linearly with the laser intensity I . Accordingly, the partial cross section obeys

$$\sigma^{n=0} \propto I^2, \quad (39)$$

in agreement with the quadratic growth seen in Fig. 2 of the main text.

The above estimate also shows that the enhancement of the $n = 0$ channel is coupled to the beam-energy asymmetry through the factor $\sqrt{p^0/q^0}$ in the amplitude. Consequently, the cross section acquires a strong dependence on the energy ratio between the electron and positron beams, consistent with the numerical behavior shown in Fig. S9.

Finally, we emphasize that the scattering cross section cannot increase indefinitely with laser intensity. At sufficiently extreme fields, the required incident energies p^0 and q^0 become comparable to the electron mass m_e , the ultrarelativistic approximations used throughout this analysis cease to be valid, and the scaling estimates derived above no longer apply quantitatively. In addition, for ultra-strong field, higher-order strong-field effects, including

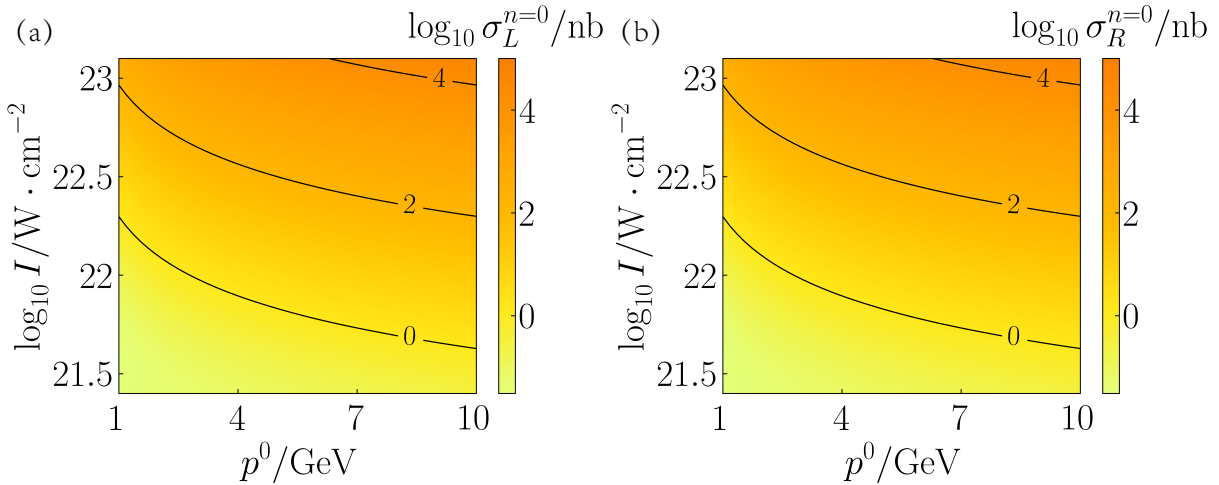


FIG. S9. The distributions of the scattering cross-section components for the $n = 0$ channel in a high-intensity laser environment, corresponding to the detailed data shown in Fig. 3 (b) and (e) in the main text at high laser intensity regime.

vacuum-polarization corrections, are expected to become important and eventually limit the growth of the amplitude.

Realistic beam effects

When the incident beams have a finite angular dispersion, the exact coaxial condition no longer holds, so that in general $p \cdot \epsilon \neq 0$ and $q \cdot \epsilon \neq 0$. In this case, the simple nonlinear picture restricted to the $n = 0, \pm 1$ channels is no longer sufficient, and additional multiphoton channels must be included, and the corresponding factor \mathcal{F}_n^λ then takes the more general form as Eq. (26). For circular polarization, we have $\not{k}\not{\epsilon} G^\lambda \not{k}\not{\epsilon} = 0$ and $\not{k}\not{\epsilon}^* G^\lambda \not{k}\not{\epsilon}^* = 0$. The nonlinear effect is thus manifested through the activation of many harmonic channels labeled by the integer n , which represents the net number of laser photons exchanged with the background field. The dominant nonlinear contribution is centered around $n \sim \alpha$, in accordance with the well-known behavior of Bessel functions.

As an example, consider a positron beam with an angular deflection $\Delta\theta_+$. To leading order, one obtains

$$\alpha = ea_0 \frac{|q \cdot \epsilon|}{q \cdot k} \approx ea_0 \frac{\Delta\theta_+}{2\sqrt{2}\omega}, \quad (40)$$

while the remaining kinematic factors can be kept at their collinear values to first order approximation. Since the Bessel functions are effectively supported in the range $|n| \lesssim \alpha$, it provides a natural truncation scale for the channel summation.

After summing statistically over all channels, the nonlinear contributions simplify substantially. Owing to angular-momentum conservation and the four-momentum-conserving delta function, channels with different photon numbers n do not interfere with each other. As a result, all cross terms between different Bessel functions vanish, and the total cross section reduces to a sum over squares of Bessel functions.

At this stage, the Neumann addition theorem [46],

$$\sum_{n=-\infty}^{\infty} J_n^2(x) = 1, \quad (41)$$

can be applied. It then follows that the summed contribution of all nonlinear channels is equal to that obtained in the simple nonlinear case, where only the $n = 0, \pm 1$ channels

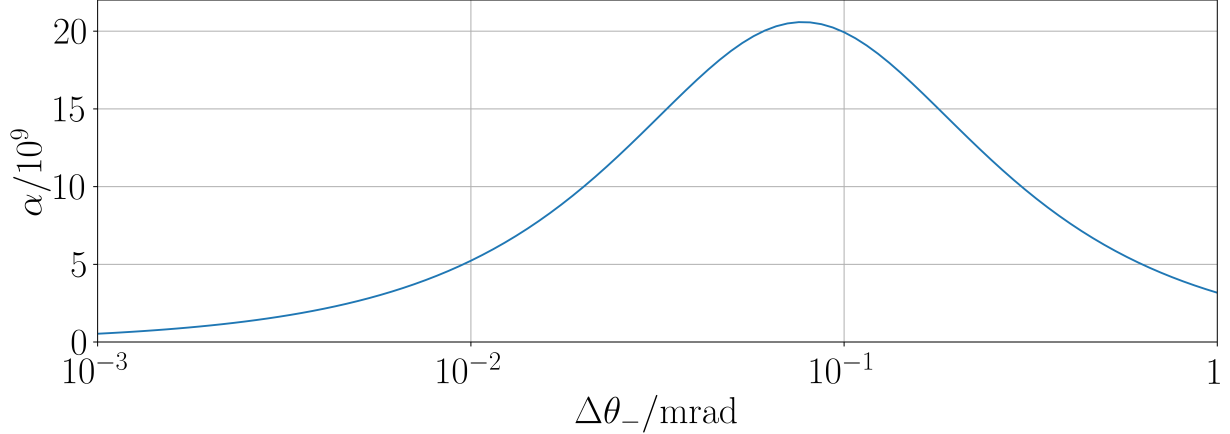


FIG. S10. The variation of parameter α when electrons have different levels of energy dispersion, which indicates the typical nonlinear exchange of photon numbers.

are retained. This conclusion remains valid provided that the exchanged photon number is much smaller to shift the resonance away from the on-shell Breit–Wigner peak, namely

$$n \ll \frac{m_Z \Gamma_Z}{\omega k_Z^0}. \quad (42)$$

For positron-beam angular deflections below the mrad level, this condition is naturally satisfied.

The situation is qualitatively different when the electron beam carries an angular dispersion $\Delta\theta_-$. In this case, the factor $p \cdot k$ itself becomes highly sensitive to the deflection angle. To leading order,

$$p \cdot k \approx \frac{m_e^2 + p_0^2 \Delta\theta_-^2}{2p^0} \omega, \quad (43)$$

so that the dependence of

$$\alpha = \frac{ea_0 |p \cdot \epsilon|}{p \cdot k} \quad (44)$$

on $\Delta\theta_-$ is no longer linear. This behavior is shown in Fig. S10 for a laser intensity of 10^{20} W/cm². At small deflection angles, the growth of α is initially driven by the linear increase of $p \cdot \epsilon$. At larger angles, however, the angular dependence of $(p \cdot k)^{-1}$ becomes dominant and suppresses α .

In contrast, for mrad-scale electron angular dispersions, the dominant nonlinear contribution corresponds to photon numbers as large as $n \sim 10^9$. Such a large number of exchanged photons carries GeV level energy, which is sufficient to drive the process away from the reso-

nant Breit–Wigner peak. There are two mechanisms contribute to the resulting deviation of the center-of-mass energy. First, the activation of extremely high-order nonlinear channels, with photon number reaching $n \sim 10^9$, perturbs the effective energy-momentum balance, as illustrated in Fig. S10. Second, and more importantly at the mrad level, the laser dressing effect is weakened because the denominator factor

$$(p \cdot k)^{-1} \approx \frac{2p^0}{(m_e^2 + p_0^2 \Delta\theta_-^2) \omega} \quad (45)$$

is highly sensitive to the electron angular deflection $\Delta\theta_-$. This reduction of the kinematic enhancement is the dominant source of the loss of resonance matching for realistic angular divergences of electron beam. At the same time, the change in the denominator factor $(p \cdot k)^{-1}$ reduces the effective coupling strength of the channel, leading to a further decrease of the yield.

We now turn from the influence of beam angular dispersion to the effect of beam energy spread. When the incoming beams have finite energy spreading, the center-of-mass energy is shifted away from the resonance condition, giving rise to a mismatch

$$\Delta s = s - m_Z^2. \quad (46)$$

For small energy deviations, the dominant contribution to this mismatch arises from the laser-induced term

$$\Delta E \sim \frac{e^2 a_0^2 q \cdot k}{p \cdot k}, \quad (47)$$

which depends linearly on the beam-energy deviation to first order. If the dressed center-of-mass energy exceeds the resonance threshold, the situation is equivalent to the laser intensity at the collision point being slightly higher than required. In practice, this can be compensated by shifting the collision point to an earlier or later position within the laser pulse envelope, where the field amplitude is weaker. Conversely, if the dressed center-of-mass energy falls below the resonance, the mismatch can be corrected by increasing the laser intensity at the collision point.

The relation between the required increase of the peak laser intensity and the tolerable downward beam-energy deviation is shown in Fig. S11(a). The result indicates that, for a typical energy spread of 0.1%, the corresponding adjustment of the laser intensity is below

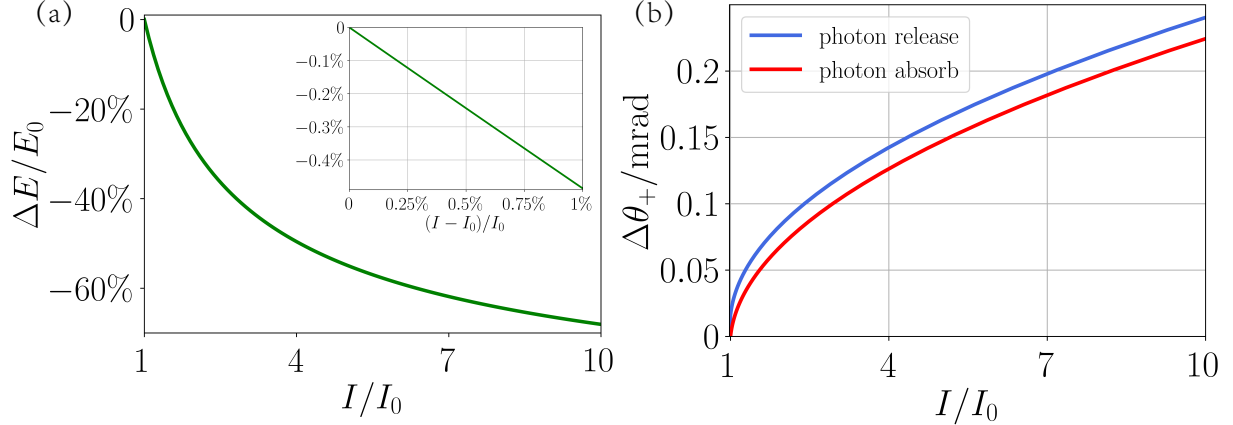


FIG. S11. Tolerance ranges of the energy spread and angular divergence of the electron beam corresponding to a one-order-of-magnitude increase in laser intensity. Panel (a) shows the case in which the electron and positron beams have the same energy spread. The low-dispersion region is enlarged in the inset, revealing an approximately linear dependence. Panel (b) shows the off-shell effect induced by beam angular divergence. The cases corresponding to the absorption and emission of $n = \pm\alpha$ laser photons are both presented.

1%. Therefore, the tolerance requirement associated with beam energy dispersion can be satisfied with only a very small tuning of the laser parameters.

Our numerical results in Fig. S11(b) show that, even when the nonlinear channels with $n \sim 10^9$ triggered by the angular dispersion of the electron beam are included, the additional laser redundancy required by these channels is not the dominant limitation. Instead, the main restriction comes from the angular dependence of the $(p \cdot k)^{-1}$ factor itself. In particular, even if the peak laser intensity is increased by one order of magnitude relative to the threshold, the electron angular spread that can be accommodated is only

$$\Delta\theta_- \approx 0.23 \text{ mrad.} \quad (48)$$

For comparison, the typical angular dispersion of the BEPCII electron beam is about 0.25 mrad [45], implying that only about 35% of the electrons in a Gaussian-distributed beam can effectively contribute to the laser-assisted resonance.

This apparent loss of usable beam particles can, however, be mitigated in several ways. Besides improving the beam emittance and reducing the angular dispersion through stronger focusing, one may also relax the constraint on the beam energy spread in order to obtain a higher beam current and hence a larger overall yield [47–49]. This tradeoff is feasible because,

as shown above, the collision scheme is much more tolerant to energy dispersion than to angular dispersion: the redundant laser intensity can efficiently compensate moderate beam-energy variations. Therefore, with suitable machine optimization, the yield loss induced by electron angular dispersion can be substantially reduced, at the price of increasing the laser intensity.

The estimation of Z Boson yield

The total Z -boson yield is given by the product of the cross section and the integrated luminosity of the accelerators. In our estimates, we adopt the cross section in the plateau regime ($\approx 2\sigma_0$). The integrated luminosity is obtained by integrating the instantaneous luminosity over the total interaction time, assuming an effective annual operation time of 10^7 sec (approximately three months). Reference luminosities and collision frequencies for representative GeV-scale colliders are summarized in Table A1.

For sub-petawatt laser systems, the typical repetition rate is currently in the kHz range. For circular colliders such as KEKB and STCF, the bunch-crossing frequency ($f_{\text{coll}} \sim 10^5$ Hz) therefore exceeds the laser repetition rate ($f_{\text{laser}} \sim 10^3$ Hz), implying that only a fraction of collisions occur in the presence of the laser field. To account for this mismatch, we introduce an effective luminosity,

$$\mathcal{L}_{\text{eff}} = \mathcal{L}_0 \min\left(1, \frac{f_{\text{laser}}}{f_{\text{coll}}}\right), \quad (49)$$

where \mathcal{L}_0 denotes the nominal collider luminosity listed in Table A1. This rescaling ensures that the estimated Z -boson yield reflects correctly the laser-synchronized collision events.

Taking these factors into account, the annual production of Z bosons can be estimated as

$$N = \sigma \mathcal{L}_{\text{eff}} \quad (50)$$

Device	Luminosity [$\text{cm}^{-2}\text{s}^{-1}$]	Collision frequency [Hz]
BEPCII [50]	10^{33}	50
KEKB [29]	10^{34}	10^5
STCF [30]	10^{34}	10^5

TABLE A1. Luminosity and collision frequency of the GeV-scale accelerators mentioned in the text.

where the integral luminosity $\mathcal{L}_{\text{eff}} = \mathcal{L}_{\text{eff}}T$ is composed of the product of effective brightness and effective working time. The estimates are obtained using the annual integrated luminosity of each facility at its representative collision energy \sqrt{s} . The effects of beam energy spread and angular dispersion are counteracted by increasing the laser intensity, thereby eliminating the impact on the overall yield. By estimating the annual Z -boson yield achievable in our setup for existing linear and circular colliders, including BEPCII, KEKB, and STCF, we compare our laser-assisting collision proposal with the projected performance of next-generation Z factories and the corresponding results are presented in table A2. The required laser intensity for each setup is also listed.

The impact of strong laser fields on the decay processes of Z Bosons

The Z boson, being a short-lived particle, decays rapidly after the generation. Its primary decay channels in vacuum are listed in Tab. A3.

Introducing a strong laser background modifies the quantum vacuum, which could in principle affect the subsequent decay of the produced Z boson. However, the massive charged particles involved in the dominant decay channels (the $b\bar{b}, c\bar{c}, \mu\bar{\mu}, \tau\bar{\tau}$ pairs) are all much heavier than electrons and positrons. And because the nonlinear effects in strong lasers scale inversely with the particle mass, the laser intensities relevant to our proposal have a negligible impact on these channels.

On the other hand, for the e^-e^+ decay channel, which is effectively the reverse of the production process, the laser-induced enhancement associated with the $(p \cdot k)^{-1}$ denominator factor is confined to a narrow micro-cone along the laser propagation axis, corresponding to a very small volume in the final phase-space of the electrons and positrons. Away from the near-axis direction, the $p \cdot k$ enhancement rapidly diminishes, further suppressing the

Device	\sqrt{s}/GeV	$I/\text{W}\cdot\text{cm}^{-2}$	Estimated annual yield
BEPCII [28]	3.78	$10^{21} - 10^{22}$	$\sim 10^{10}$
KEKB [29]	10.6	$10^{20} - 10^{21}$	$\sim 10^8$
STCF [30]	4	$10^{21} - 10^{22}$	$\sim 10^8$
CEPC [51]	91.2	-	$\sim 10^{12}$

TABLE A2. Estimated annual Z -boson yields for the laser-assisted scheme using existing accelerator facilities. The typical collision energy \sqrt{s} of the device and the required laser intensity I are both listed together. The expected yield from the CEPC proposal is shown for comparison.

Decay products	Ratio	Product mass	Product charge
light quark pairs	$\sim 50\%$	$2 \sim 5 \text{ MeV}$	$\pm 1/3$ or $\pm 2/3$
$b\bar{b}$ pairs	$\sim 10\%$	4.2 GeV	$\pm 1/3$
$c\bar{c}$ pairs	$\sim 8\%$	1.3 GeV	$\pm 2/3$
e^-e^+ pairs	$\sim 3\%$	0.5 MeV	± 1
$\mu\bar{\mu}$ pairs	$\sim 3\%$	105.6 MeV	± 1
$\tau\bar{\tau}$ pairs	$\sim 3\%$	1.8GeV	± 1
neutrino pairs	$\sim 20\%$	0	0

TABLE A3. The decay channels and decay product properties of the Z boson in a vacuum [52–56].

laser influence. The light-quark channels experience a similar effect, but the impact is further reduced—by roughly two orders of magnitude—because the quark masses exceed the electron mass by about one order of magnitude, and their total contribution is likewise limited by the small near-axis phase-space region.

Consequently, we conclude that the effect of the laser background on the total decay width of the Z boson is negligible.

* qzlv@gscaep.ac.cn

† lbfu@gscaep.ac.cn

- [1] S. Schael, R. Barate, R. Bruneliere, D. Buskulic, B. De, D. Decamp, P. Ghez, C. Goy, S. Jezequel, J. Lees, *et al.*, Precision electroweak measurements on the Z resonance, [Physics Reports](#) **427**, 257 (2006).
- [2] M. Martinez, R. Miquel, L. Rolandi, and R. Tenchini, Precision tests of the electroweak interaction at the z pole, [Rev. Mod. Phys.](#) **71**, 575 (1999).
- [3] K. Abe, K. Abe, T. Abe, I. Adam, H. Akimoto, D. Aston, K. Baird, C. Baltay, H. Band, T. Barklow, *et al.*, High-precision measurement of the left-right z boson cross-section asymmetry, [Physical review letters](#) **84**, 5945 (2000).
- [4] T. Kawamoto and R. G. Kellogg, Character of z-pole data constraints on standard model parameters, [Phys. Rev. D](#) **69**, 113008 (2004).
- [5] L. Allwicher, M. McCullough, and S. Renner, New physics at Tera-Z: precision renormalised, [Journal of High Energy Physics](#) **2025**, 164 (2025).
- [6] A. Falkowski and F. Riva, Model-independent precision constraints on dimension-6 operators,

- Journal of High Energy Physics **2015**, 1 (2015).
- [7] A. Bohm, H. Kaldass, and S. Wickramasekara, Time asymmetric quantum theory – II. Relativistic resonances from S-matrix poles, [Fortschritte der Physik](#) **51**, 569 (2003).
 - [8] working group on LEP energy, R. Assmann, A. Beuret, A. Blondel, J. Billan, R. Billen, G. Bobbink, F. Bordry, H. Burkhardt, B. Dehning, *et al.*, The energy calibration of lep in the 1993 scan, [Zeitschrift für Physik C Particles and Fields](#) **66**, 567 (1995).
 - [9] G. Panico, Precision measurements at future colliders, [PoS CORFU2024](#), 049 (2025).
 - [10] M. Benedikt, F. Zimmermann, B. Auchmann, W. Bartmann, *et al.* (FCC), Future Circular Collider Feasibility Study Report Volume 2, [Eur. Phys. J. Spec. Top.](#) , 5713 (2025), [arXiv:2505.00274](#).
 - [11] T. C. S. Group, [Cepc technical design report – reference detector](#) (2025), [arXiv:2510.05260 \[hep-ex\]](#).
 - [12] A. Fedotov, A. Ilderton, F. Karbstein, B. King, D. Seipt, H. Taya, and G. Torgrimsson, Advances in QED with intense background fields, [Physics Reports](#) **1010**, 1 (2023), advances in QED with intense background fields.
 - [13] A. Gonoskov, T. G. Blackburn, M. Marklund, and S. S. Bulanov, Charged particle motion and radiation in strong electromagnetic fields, [Rev. Mod. Phys.](#) **94**, 045001 (2022).
 - [14] A. Di Piazza, C. Müller, K. Z. Hatsagortsyan, and C. H. Keitel, Extremely high-intensity laser interactions with fundamental quantum systems, [Reviews of Modern Physics](#) **84**, 1177 (2012).
 - [15] V. I. Ritus, Quantum effects of the interaction of elementary particles with an intense electromagnetic field, [Journal of Soviet Laser Research](#) **6**, 497 (1985).
 - [16] D. M. Wolkow, Über eine Klasse von Lösungen der Diracschen Gleichung, [Z. Angew. Phys.](#) **94**, 250 (1935).
 - [17] A. Di Piazza, Ultrarelativistic electron states in a general background electromagnetic field, [Physical review letters](#) **113**, 040402 (2014).
 - [18] A. Di Piazza, Completeness and orthonormality of the volkov states and the volkov propagator in configuration space, [Physical Review D](#) **97**, 056028 (2018).
 - [19] C. F. Nielsen, R. Holtzapple, M. M. Lund, J. H. Surrow, A. H. Sørensen, M. B. Sørensen, U. I. Uggerhøj, and C. NA63), Precision measurement of trident production in strong electromagnetic fields, [Physical Review Letters](#) **130**, 071601 (2023).
 - [20] C. Kohlfürst, N. Ahmadienia, J. Oertel, and R. Schützhold, Sauter-schwinger effect for collid-

- ing laser pulses, *Physical Review Letters* **129**, 241801 (2022).
- [21] Y.-F. Li, Y.-Y. Chen, K. Z. Hatsagortsyan, and C. H. Keitel, Helicity transfer in strong laser fields via the electron anomalous magnetic moment, *Physical Review Letters* **128**, 174801 (2022).
- [22] K. Xue, T. Sun, K.-J. Wei, Z.-P. Li, Q. Zhao, F. Wan, C. Lv, Y.-T. Zhao, Z.-F. Xu, and J.-X. Li, Generation of high-density high-polarization positrons via single-shot strong laser-foil interaction, *Physical Review Letters* **131**, 175101 (2023).
- [23] S. Tang, Fully polarized nonlinear breit-wheeler pair production in pulsed plane waves, *Physical Review D* **105**, 056018 (2022).
- [24] D. Seipt, C. P. Ridgers, D. Del Sorbo, and A. G. Thomas, Polarized qed cascades, *New Journal of Physics* **23**, 053025 (2021).
- [25] See the Supplemental Materials for the detailed derivation and analysis.
- [26] A. Di Piazza, C. Müller, K. Z. Hatsagortsyan, and C. H. Keitel, Extremely high-intensity laser interactions with fundamental quantum systems, *Rev. Mod. Phys.* **84**, 1177 (2012).
- [27] M. Tanabashi, K. Hagiwara, K. Hikasa, *et al.* (Particle Data Group), Review of Particle Physics, *Phys. Rev. D* **98**, 030001 (2018).
- [28] H. Shi, B. Wang, H. Shi, C. Yu, M. Dong, and H. Peng, Beam background simulation and experiment at BEPCII, *Nuclear Instruments and Methods in Physics Research Section A: Accelerators, Spectrometers, Detectors and Associated Equipment* **1050**, 168174 (2023).
- [29] P. Branchini, The Belle II Experiment: Status and Prospects, *Universe* **4**, 101 (2018).
- [30] X.-C. Ai, L.-P. An, S.-Z. An, *et al.*, Conceptual design report of the Super Tau-Charm Facility: the accelerator, *Nuclear Science and Techniques* **36**, 242 (2025).
- [31] Y. Zhao, F. Wu, C. Wang, J. Hu, *et al.*, Spatiotemporal aberrations due to the groove density mismatching of compression gratings in ultra-intense femtosecond lasers, *Scientific Reports* **14**, 18231 (2024).
- [32] Z. Major, U. Eisenbarth, B. Zielbauer, C. Brabetz, J. B. Ohland, Y. Zobus, S. Roeder, D. Reemts, S. Kunzer, S. Götte, and *et al.*, High-energy laser facility PHELIX at GSI: latest advances and extended capabilities, *High Power Laser Science and Engineering* **12**, e39 (2024).
- [33] Y. Han, Z. Li, Y. Zhang, F. Kong, H. Cao, Y. Jin, Y. Leng, R. Li, and J. Shao, 400nm ultra-broadband gratings for near-single-cycle 100 Petawatt lasers, *Nature Communications* **14**, 3632 (2023).

- [34] S. Du, X. Shen, W. Liang, P. Wang, J. Liu, and R. Li, A 100-PW compressor based on single-pass single-grating pair, [High Power Laser Science and Engineering](#) **11**, e4 (2023).
- [35] Z. Guo, L. Yu, J. Wang, C. Wang, Y. Liu, Z. Gan, W. Li, Y. Leng, X. Liang, and R. Li, Improvement of the focusing ability by double deformable mirrors for 10-PW-level Ti: sapphire chirped pulse amplification laser system, [Opt. Express](#) **26**, 26776 (2018).
- [36] H. Mimura, H. Yumoto, S. Matsuyama, T. Koyama, K. Tono, Y. Inubushi, T. Togashi, T. Sato, J. Kim, R. Fukui, Y. Sano, M. Yabashi, H. Ohashi, T. Ishikawa, and K. Yamauchi, Generation of 10^{20}Wcm^{-2} hard X-ray laser pulses with two-stage reflective focusing system, [Nature Communications](#) **5**, 3539 (2014).
- [37] W. H. Furry, On Bound States and Scattering in Positron Theory, [Phys. Rev.](#) **81**, 115 (1951).
- [38] M. Hoferichter, J. Menéndez, and A. Schwenk, Coherent elastic neutrino-nucleus scattering: EFT analysis and nuclear responses, [Phys. Rev. D](#) **102**, 074018 (2020).
- [39] G. Breit and E. Wigner, Capture of Slow Neutrons, [Phys. Rev.](#) **49**, 519 (1936).
- [40] M. Maggiore, *A Modern Introduction to Quantum Field Theory* (Oxford University Press, 2004).
- [41] M. E. Peskin, *An Introduction to Quantum Field Theory*, 1st ed. (CRC Press, Boca Raton, 1995).
- [42] W. Shu-Hong, P. Guo-Xi, C. Yun-Long, C. Yan-Wei, C. Jian-She, K. Xiang-Cheng, Z. Feng-Li, H. Mi, C. Zhi-Bi, L. Wei-Bin, D. Bing-Lin, G. Zhe-Qiao, P. Shi-Lun, S. Li, L. Qi, and Y. Qiang, Bepcii linac beam commissioning and operation, [Chinese Physics C](#) **32**, 215 (2008).
- [43] T. Suwada, M. Satoh, and K. Furukawa, Nondestructive beam energy-spread monitor using multi-strip-line electrodes, [Phys. Rev. ST Accel. Beams](#) **6**, 032801 (2003).
- [44] O. Kononenko and A. Grudiev, Transient beam-loading model and compensation in compact linear collider main linac, [Phys. Rev. ST Accel. Beams](#) **14**, 111001 (2011).
- [45] W. Shu-hong, G. Peng-da, L. Wei-bin, and P. Shi-lun, [Error and jitter effects on BEPII-linac](#) (2005).
- [46] G. N. Watson, *A Treatise on the Theory of Bessel Functions*, 2nd ed. (Cambridge University Press, Cambridge, 1944) chap. XI.
- [47] M. Eshraqi and J. Lagniel, Choice of linac parameters to minimize the space-charge effects, [Journal of Instrumentation](#) **15** (07), P07024.
- [48] F. Zimmermann, M. Korostelev, D. Schulte, T. Agoh, and K. Yokoya, Collective Effects in

- the CLIC Damping Rings, in *Proceedings of the 2005 Particle Accelerator Conference* (IEEE) p. 1312–1314.
- [49] S. Dastan, D. Zhou, T. Ishibashi, E. Karantzoulis, S. Di Mitri, and R. Lindberg, Coherent synchrotron radiation instability in low-emittance electron storage rings, *Phys. Rev. Accel. Beams* **27**, 104401 (2024).
- [50] J. Gao, CEPC Technical Design Report: Accelerator, *Radiation Detection Technology and Methods* **8**, 1 (2024).
- [51] H. Liang, Y. Zhu, P.-Z. Lai, and M. Ruan, Optimization of tracker configuration for the cepec, *Journal of Instrumentation* **17** (11), P11016.
- [52] G. Aad, B. Abbott, D. C. Abbott, A. A. Abud, K. Abeling, *et al.*, Search for charged-lepton-flavour violation in Z-boson decays with the ATLAS detector, *Nature Physics* **17**, 819 (2021).
- [53] A. M. Sirunyan, A. Tumasyan, W. Adam, T. Bergauer, M. Dragicevic, A. Escalante Del Valle, *et al.*, Measurement of the Z boson differential production cross section using its invisible decay mode ($Z \rightarrow \nu\bar{\nu}$) in proton-proton collisions at $\sqrt{s}=13$ TeV, *Journal of High Energy Physics* **2021**, 205 (2021).
- [54] I. Dubovyk, A. Freitas, J. Gluza, T. Riemann, and J. Usovitsch, Electroweak pseudo-observables and Z-boson form factors at two-loop accuracy, *Journal of High Energy Physics* **2019**, 113 (2019).
- [55] A. Freitas, Higher-order electroweak corrections to the partial widths and branching ratios of the Z boson, *Journal of High Energy Physics* **2014**, 70 (2014).
- [56] G. Abbiendi, C. Ainsley, P. Åkesson, G. Alexander, J. Allison, *et al.*, Charged particle multiplicities in heavy and light quark initiated events above the Z0 peak, *Physics Letters B* **550**, 33 (2002).